MADRID
inter.noise 2019
June 16 - 19
NOISE CONTROL FOR A BETTER ENVIRONMENT

Monitoring infrastructure asset through its acoustic signature

Fedele, Rosario[1]
University Mediterranea of Reggio Calabria
Via Graziella, 89124, Reggio Calabria (RC), Italy

Praticò, Filippo Giammaria[2]
University Mediterranea of Reggio Calabria
Via Graziella, 89124, Reggio Calabria (RC), Italy

ABSTRACT

Structural health monitoring can benefit transportation infrastructures in terms of pavement management systems and risk management. In this study, a new, non-destructive, acoustic-based method for assessing and monitoring the structural health status (SHS) of road pavements along their operational life is presented. In order to validate the proposed method, an experimental investigation was carried out. The acoustic response of an asphalt concrete road pavement following a proper mechanical excitation (hereafter named acoustic signature) was recorded and analysed. A specifically designed microphone-based electronic system was set up and applied. The acoustic responses were analysed in the time and frequency domain. An integrated system, including the power supply, the abovementioned system, and data transmission equipment was set up and applied as a part of a research project, to collect data and extract features and information valuable to different stakeholders. Experimental results show that the proposed system is able to detect the change of the acoustic signature of the infrastructure asset over time using a small number of meaningful features extracted by clustering techniques. Consequently, it can be used to monitor the SHS of road pavements by detecting the onset of cracks, and keeping under observation their evolution over time.

Keywords: Acoustic signature, intelligent structural health monitoring, feature-based hierarchical clustering
I-INCE Classification of Subject Number: 74
http://i-ince.org/files/data/classification.pdf

1. INTRODUCTION

During its life time, a road pavement is subjected to repeated thermal and vehicular traffic loads. These loads induce stresses, strains, displacements, and vibrations into the pavement layers. These effects lead to the generation and propagation of several types of cracks until the failure of the road pavement occurs. Many methods have been proposed in the last decades in order to carry out the assessment and monitoring of the structural conditions of road infrastructures in real conditions (e.g., under traffic-related stresses),

[1] rosario.fedele@unirc.it
[2] filippo.pratico@unirc.it

or under simulated stresses. Importantly, different factors should be taken into account when road pavements need to be monitored. These factors mainly refer to: i) the sources of the above-mentioned stresses, which in turn are function of vehicle-, and traffic-related features [1]; ii) the mean of propagation of traffic-induced stresses (i.e., the pavement) and its properties, performance, and conditions [2–6].

Road pavement Structural Health Monitoring (SHM) usually aims at detecting surface cracks and rarely internal cracks. Tests and particularly Non-Destructive Tests (NDT) use different types of sensors([7]), vehicles equipped with cameras [8], laser scanners [8,9], vehicles equipped with three-axis accelerometers [10], with smartphone gyroscopes [11–13], or accelerometers embedded or placed on the road surface [14,15]. Internal cracks can be monitored using Ground Penetrating Radars (GPR; see e.g., [16]).

Intelligent solutions should be able to detect, in real-time, changes of the response of a monitored road pavement to stresses and loads. To this end, a SHM system may need to: i) identify variations of the signals collected; ii) recognize signals variations over time; iii) derive the frequency components corresponding to the variations above; iv) detect the "development" of new frequencies in the signals due to changes in the structural dynamics [17]. In the last decades, different Intelligent Transportation System (ITS)-based and/or SHM-based systems, with different data processing methods have been proposed, among which filter-based methods [18], Gabor filter [19], Artificial Neural Network (ANN; cf. e.g., [20,21], Wavelet Transform (WT) [17,22,23], or ANN combined with WT [9,12,24–26]. Despite the high number of methods proposed, solutions are still needed to promptly detect "invisible" (bottom-up) structural failures, which are crucial for flexible pavements [27].

Based on preliminary studies [28,29], the study presented in this paper aims at solving some of the issues listed above (see Section 2). Section 3 deals with the description of method and experimental set-up. Section 4 deals with the results and is followed by Conclusions.

2. OBJECTIVES

Based on previous section, the main objectives of this study are:

1) to present an innovative SHM method, specially designed for road pavements, which is based on signal analysis.
2) to carry out a prototypical validation of the method, dealing with controlled impulses.

3. METHOD AND EXPERIMENTAL SET UP

In this study, a cheap, simple, and NDT method for detecting underneath cracks and allowing an intelligent road monitoring is presented. This method (see Figure 1) is innovative and considers: 1) waves originated by mechanical sources (e.g., the vehicular traffic); 2) the road pavement as a "filter" of waves (i.e., vibrations and sounds); 3) waves gathered using a proper receiver (i.e., a probe that acts as a stethoscope). Any variation of the responses cited above is associated to a variation of the filter. 4) Consequently, any variation of this particular filter (e.g., due to the occurrence, or the propagation of concealed distresses) may be used to identify the structural health status variations of road pavements. Based in the above, the proposed method consists of the following steps:

Step 1: The probe (a microphone isolated from the air-borne noise) is installed (NDT).
Step 2: The acoustic responses of the pavement (sounds) are recorded.
Step 3: The acoustic data gathered during the previous step are properly processed.
Step 4: The features extracted are analysed over (hierarchical clustering, HC).

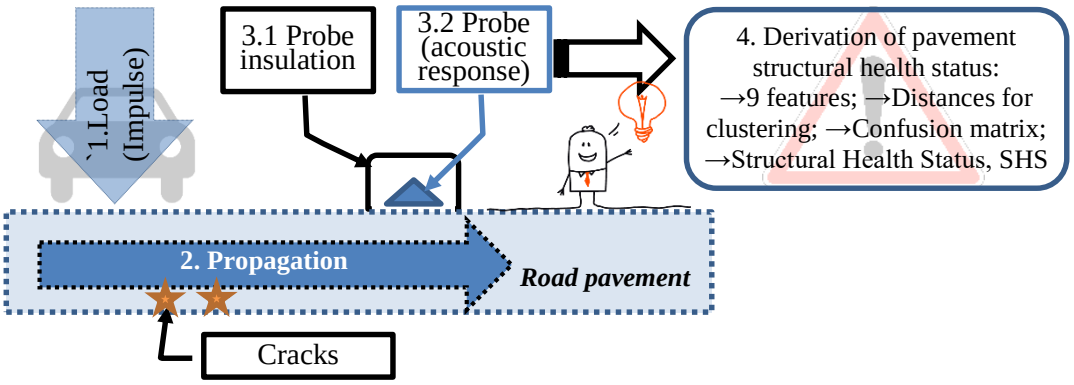

Figure 1. Schematic of the method.

Authors carried out full-scale experiments. In more detail: i) the temperatures of air and road surface were measured; ii) different structural health statuses (SHSs) were induced (drilled holes); iii) a broad-band omnidirectional microphone (see Figure 2), equipped with an external sound card, was used as a probe to gather the acoustic responses of the pavement in each SHS. The probe was attached on the road pavement using modelling clay and was covered with a cover with an high sound absorbing coefficient (in order to isolate the probe from the air-born noise, and minimize the disturbances due to the wind); iv) a Light Weight Deflectometer (LWD; Model: PRIMA100, produced by Grontmij, Carl Bro A/S, Pavement Consultants, Denmark; see Figure 2), and a car were used as sources to generate loads and waves; v) a laptop running Matlab was used to record, process, and analyse the acoustic data gathered during the experiments. Note that this paper refers on the measurements carried out using the LWD as a source only.

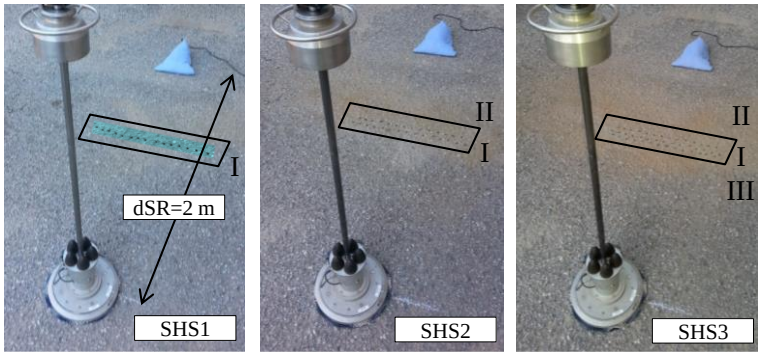

(a) (b) (c)

Figure 2. Experimental set up using the LWD as source: different structural health statuses (SHSs) of the road pavement under test, which was damaged with: (a) 1 line of drilled holes (=SHS1), (b) 2 lines of holes (=SHS2), and 3 lines of holes (=SHS3).

It is important to underline that, the LWD is a device primarily used to evaluate the dynamic modulus of pavements (usually unbound layers) according to the standard ASTM E 2583-07 [30]. Usually, during the test carried out using the most common LWDs [31], the pavement is loaded with an impulse (i.e., maximum applied force = 7-20 kN, total load pulse = 15-30 ms, plate diameter = 100-300 mm, pressure about 100 kPa) generated by a fixed mass (i.e., 2-15 kg), dropped from a fixed height (i.e., 60-85 cm). The mechanical energy is transferred from the mass to the pavement (the measurement depth is 1-1.5 times the LWD plate diameter; cf. [32]) through a damping system, which causes a controlled transient load in the interface plate-pavement. The resulting road

surface deflection in the interface pavement-plate is detected by one accelerometer located into the LWD base. Forces and deflections are used to derive the stiffness, also called modulus or dynamic modulus, of the underneath pavement layers (about 2 times the diameter of the base plate [33]).
During the experimental investigation, it has been noticed that the metallic plate of the LWD often generates undesirable sound components, which, in case of unsatisfactory insulation of the microphone, might worsen SHS classification. To solve this problem, different systems were tested to set up a proper coupling between the metallic plate and the road surface. Good results were obtained using thin layers of modelling clay, rubber mats, or cloth disc.
The first set of 50 Acoustic Responses (ARs) of the pavement that were recorded during the experimental investigation, refers to SHS0, i.e., to the road pavement without drilled holes. The signals were recorded running a simple Matlab code and using a sampling frequency of 192 kilo Samples/second. As is well known, the main effects of the vehicles wheels (especially of the heavy ones) on a road lane can be localized, into the wheel paths [27,34]. Overall, it is possible to assume that the change of the SHS of the road pavement is likely to be assessed by referring to the wheel path volumes (deep layers), i.e., where it is more probable to detect concealed cracks. Consequently, in order to simulate the presence of cracks along the wheel paths, three lines of holes were drilled between the source (wheel paths) and the receiver (i.e., half of the distance LWD-microphone, herein called dSR). In more detail, 43 holes were drilled as follows (see Figure 2): i) the first line of 15 holes was drilled at half of the distance dSR; ii) the second line of 14 holes was drilled between the first line of holes and the microphone, in such a way to obtain distances among the holes of approximately 5 cm (i.e., a group of three neighbour holes forms an equilateral triangle); iii) the third line of 14 holes was drilled between the LWD and the first line of holes. Each hole has a diameter of 10 mm, and a height equal to the thickness of the asphalt concrete layers of the pavement (i.e., 15 cm). The 43 holes were made with a distance of 5 cm from each other. After the creation of each of the 43 holes, 50 loads were generated with the LWD and the related 50 ARs of the pavement were recorded. At the end of the experiment, 2200 ARs were collected.

Figure 3 illustrates typical signals in time domain for a LWD (Figure 3a) and for a car (Figure 3b). As abovementioned, the study presented in this paper mainly refers to the prototypical validation of the method under controlled conditions. Consequently, only LWD signals are discussed below and used in the subsequent SHS classification.

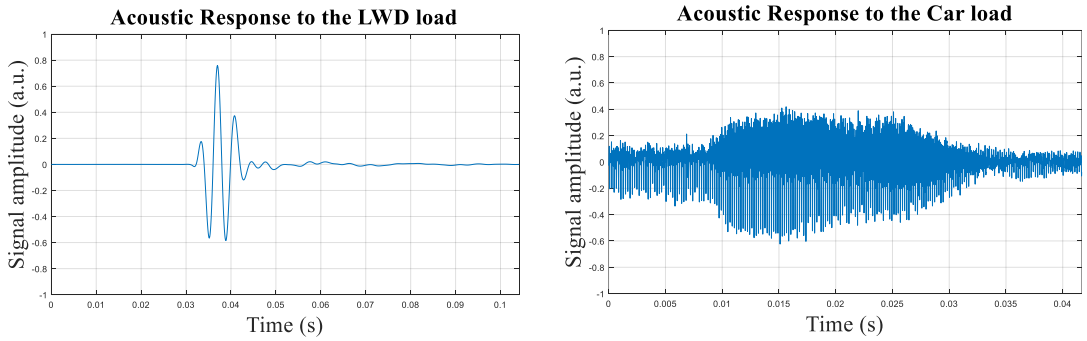

Figure 3. Examples of the Acoustic Responses (ARs) of the road pavement under test to loads generated by: (a) LWD; and (b) a car pass-by.

Preliminary analyses showed that the acoustic signals were too complex and large to use without preliminary processing. In order to carry out a comprehensive analysis, the features were extracted from the time, the frequency, and time-frequency domain. Several features were taken into account considering the shape and the main characteristics of the Acoustic Responses (ARs) of the pavement under test (time domain), and their processing (i.e. periodogram and scalogram in frequency and time-frequency domains, respectively). Among all the possible features, we selected the best three ones for each domain, which are listed in Table 1.

Table 1. Features that were taken into account in this study to represent the acoustic responses of the road pavement under test to the LWD load.

Symbol	Feature	Unit of measure	Domain / Feature Source
1. Δa	Amplitude difference between the absolute maximum P and the absolute minimum N of the AR amplitudes.	a.u.	Time / Signal
2. Δt	Time Delay of N from P	Ms	
3. σ	Standard deviation of the ARs.	a.u.	
4. PSD_{min}	Minimum of the PSD of the ARs into the frequency range 50-150 Hz.	dBW/Hz	Frequency / Periodogram
5. S	Slope of the linear regression model of the PSD of the ARs into the frequency range 20-250 Hz.	Hz	
6. f_c	Spectral Centroid of the Periodogram (PSD vs. frequency) in the frequency range 20-450 Hz.	Hz	
7. Ent_{CWCs}	Maximum Entropy of the CWCs.	a.u.	Time-Frequency / CWT Scalogram
8. $p\text{-}f_{WR}$	Pseudo-frequency of the WR (from the y-axis of the scalogram).	Hz	
9. $Eng_{CWCs,max}$	Energy of the CWCs above a given threshold (60 out of 64, i.e. red areas of the Scalogram).	a.u.	

Symbols. AR = Acoustic Response; a.u. = arbitrary unit; dim. = dimensionless; ms = milliseconds; dB = decibel; dBW/Hz = decibel Watt per Hertz; Hz = Hertz; s = seconds; Ent = Entropy; CWCs = Continuous Wavelet Coefficients; *p-f* = pseudo-frequency; WR = Wavelet Ridges; Eng = Energy; max =maximum; min = minimum.

Figure 4 refers to two out of the three features extracted in time domain.

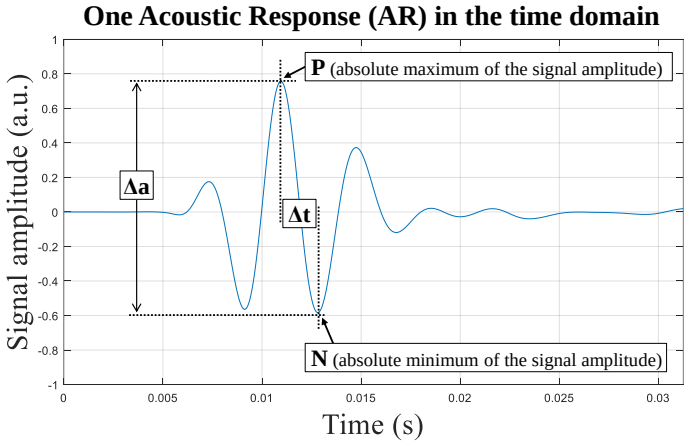

Figure 4. Graphical representation of two features extracted in the time domain.

In order to derive the three features in the frequency domain, the periodogram (Power Spectral Density versus Frequency; see Figure 5) of each AR was obtained using the following equation [35]:

$$PSD = 2 \cdot \frac{|FFT|^2}{N \cdot Fs} \ , \tag{1}$$

where FFT is the Fast Fourier Transform of the selected response; *N* is the length of the selected response (samples); *Fs* is the sample frequency used to record the signals (Hz). *PSD* is the power of the AR per unit of frequency, i.e., Watt per Hertz or dBW/Hz if the decibel scale is used to represent the PSD. In this study, in the pursuit of better analysing the PSD of the ARs of the pavement under investigation, the logarithmic scale for the y-axis (dBW/Hz) was used and values between -100 and 0 (y-axis) and in the range 25-450 (x-axis) were considered (Fig. 4). Furthermore, the periodogram in Fig. 4 shows: i) the section of the periodogram where the local minima of PSD were calculated (i.e., the feature herein called PSDmin); ii) an example of linear regression line of the PSD into the frequency range 20-250 Hz and its slope (i.e., the feature herein called S, cf. Table 1); iii) the spectral centroids of the periodogram (i.e., the feature herein called fc, which is represented by a triangle). From the periodogram, the spectral centroid ("centre of mass" of the periodogram, cf. [36]) was derived using the following expression:

$$f_c = \frac{\sum_{n=0}^{N-1} p_n \cdot f_n}{\sum_{n=0}^{N-1} p_n}, \tag{2}$$

where *fc* is the spectral centroid (Hz); *N* is the number of signal samples included in the frequency range in which the spectral centroid is calculated (samples); p_n represents the weights (e.g. decibel Watt per Hz or dBW/Hz), i.e., the values on the y-axis of the periodogram; *fn* refers to the frequencies (Hz; x-axis of the periodogram).

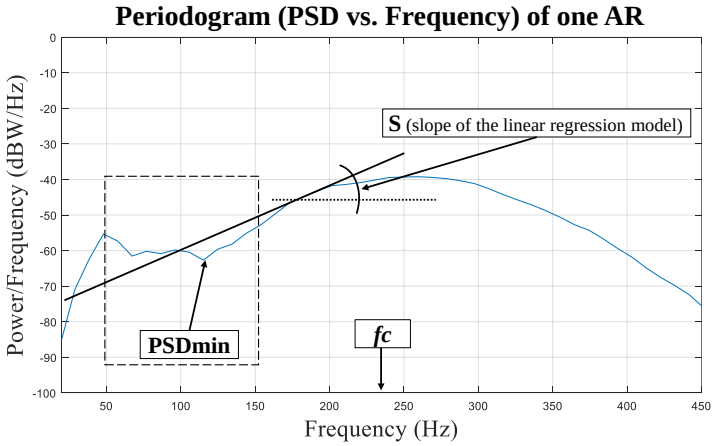

Figure 5. Graphical representation of the features used in the frequency domain.

Wavelet transforms resulted to be the most suitable method to see signal changes because of the well-known property called "time-frequency localization" [17,37]. This is the main strength of the WT, which makes the WT: i) more similar to the human ear than

other “too much artificial” tools; ii) particularly suitable for the recognition and the monitoring of non-stationary phenomena or of signals with short-lived transient components (which are the combination of transient high frequency components - visible at the top of the scalogram - and long lasting low frequency components - shown at the bottom of the scalogram as a continuous magnitude; [37]). For these reasons, the WT were used in this study. In particular, the Continuous Wavelet Transform (CWT) was preferred to the Discrete Wavelet Transform (DWT) because of the fact it allows more detailed analysis than the DWT. The results of the application of the CWT (Equation 3) is a matrix that contain the Continuous Wavelet Coefficients (CWCs), which are the result of the convolution between the signal to be analysed and a variable-sized window functions called Wavelet (or mother wavelet; cf. [37]). A typical 2-D graphical representation of the CWCs in the time-frequency domain is the “scalogram” (see Figure 6). It shows the scaled percentage of energy of the wavelet coefficients (different colours or intensity variation of a colour) with respect to time, or shift (x-axis), and scale variables (y-axis) [17].

$$CWT(a,b) = \frac{1}{\sqrt{a}} \int x(t) \cdot \psi^* \left(\frac{t-b}{a} \right) dt \,, \tag{3}$$

where a is the scaling parameter (a vector with positive elements, which allows contracting the mother wavelet ψ [38]); b is the shifting parameter, which permits the translation of the mother wavelet ψ along the x-axis (time); $x(t)$ is the signal to be transformed; t stands for time (seconds); ψ^* is the complex conjugate of ψ. Usually, scalograms show on the y-axis the scaling parameter, a. However, in this work, a pseudo-frequency was derived from the scaling parameter using the following expression [39]:

$$F_a = \frac{F_c}{a} \cdot F_S \,, \tag{4}$$

where Fa is the pseudo-frequency (Hz) corresponding to the scale factor a (dimensionless); Fc is the central frequency of the mother wavelet ψ used (Hz); F_S is the sampling frequency (Hz). In this study, the mother wavelet “meyr” was used in the CWT.

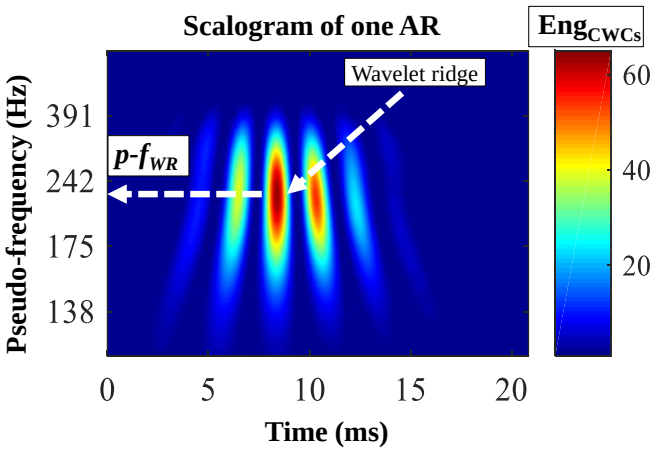

Figure 6. Graphical representation of two features used in the time-frequency domain.

The features extracted in the time-frequency domain were derived from the scalograms and from the CWCs as follows. The Shannon's Entropy of the CWCs (herein called Ent_{CWC}) per each scale factor a was calculated using the following expression [40]:

$$Ent_{CWC}(a) = -\sum_{i=1}^{N} p_i \cdot \log_2 p_i \text{, with } p_i = \frac{|CWC(a,i)|^2}{Eng(a)}, \quad (5)$$

where N is the length of each AR, and pi is the energy probability distribution of the CWCs, for i = 1, 2, …, N. The term $Eng_{CWC}(a)$ represents the Energy of the CWCs per each scale factor a. In more detail [40], the variable $Eng_{CWC}(a)$ can be calculated from the CWCs, for b = 1, 2, …, N (with N equal to the length of each AR), using the following expression:

$$Eng_{CWC}(a) = \sum_{b} |CWC(a,b)|^2. \quad (6)$$

Finally, the validation of the method proposed in this study is based on the experimental investigation described above and on the following procedure that aims at carrying out the hierarchical clustering of the acoustic responses (ARs) of the road pavement and the relative features presented above. In particular, this procedure consists in: i) computing the distance matrix, which contains the Euclidean distances between pairs of observations (i.e., samples of each AR or values of each features) [41]; ii) encoding a tree of hierarchical clusters (i.e., a matrix with cluster indices and linkage distances between pairs of clusters) using as input the distance matrix calculated in the first step, counting the highest distance between two element of the distance matrix, and considering 4 clusters, i.e., one for the structural health condition un-cracked, and the other three for the structural health status (SHS) cracked with one, two, and three lines of holes drilled into the road pavement under investigation; iii) finding the smallest height at which a horizontal cut through the agglomerative hierarchical cluster tree (generated in the previous step) groups the observations into 4 clusters; iv) generating the confusion matrix (i.e., a matrix that shows how many observations were associated to each cluster) and verifying if the ARs associated to a given SHS is correctly clustered and associated to a single cluster.

4. RESULTS AND DISCUSSIONS

Results are given in Tables 2-3. Table 2 contains the values of the features extracted in the three domains of analysis (time, frequency, and time-frequency). It shows how the abovementioned features change when the Structural Health Status (SHS) of the road pavement gets worse, i.e., moves from SHS0 (un-cracked pavement) to SHS3 (road pavement cracked with 3 lines of holes).

Table 2. Values of all the features used in this study.

Symbol	SHS0	SHS1	SHS2	SHS3	Symbols. SHSi = i-th Structural Health Status of the road pavement under test, with i=0, ..., 3; a.u. = arbitrary unit; dim. = dimensionless; ms = milliseconds; dB = decibel; dBW/Hz = decibel Watt per Hertz; Hz = Hertz; Ent = Entropy; CWCs = Continuous Wavelet Coefficients; *p-f* = pseudo-
Δa [a.u.]	1.34	1.44	1.35	1.28	
Δt [ms]	**1.86**	**1.81**	**1.72**	**1.70**	
σ [a.u.]	13.21%	13.91%	13.32%	12.55%	
PSD_{min} *[dBW/Hz]*	-51.6	-52.6	-54.9	-55.6	
S [dBW]	0.132	0.134	0.130	0.127	
f_c *[Hz]*	239	242	250	254	
Ent*$_{CWCs}$ *[a.u.]	**11.54**	**11.76**	**11.90**	**11.93**	

$p\text{-}f_{WR}$ *[Hz]*	262	280	284	287	frequency; WR = Wavelet Ridges; Eng = Energy; max =maximum; min = minimum.
$Eng_{CWCs,max}$ *[a.u.]*	2.61%	1.97%	1.88%	2.14%	

Based on Table 2, the following observations can be made: i) The presence and the increase of the number of cracks into the road pavement seems to lead to a dissipation of the energy of the sound and of the seismic waves traveling from the source, through the road pavement, to the receiver. This dissipation is caused by the complex interactions (adsorption, reflection and diffraction) between the mechanical waves and the drilled holes. This statement was derived observing the reduction of the features Δa, σ, and $Eng_{CWCs,max}$, and the increase of the Shannon's Entropy of the CWCs (which represents the increase of the chaos of the system); ii) From a spectral point of view, the dissipation of the energy discussed above can be seen as a reduction of some spectral components in the low frequency region, which leads to an increase of the influence of the high frequency belonging to the same region. These conclusions were derived by analysing the trends of the features Δt, *PSDmin*, *S*, *fc* and $Eng_{CWCs,max}$.

Despite the considerations reported above, it seems quite difficult to validate the proposed method, i.e., to demonstrate that it is possible to recognize the variation of the SHS of the road pavement using only the trends of the feature extracted. For this reason, the hierarchical clustering procedure defined above was used. Confusion matrixes were used to express the results of the clustering procedure. As is well-known, the instances in a predicted class are represented in each row of the confusion matrix, while the instances in an actual class are reported in each column of the matrix (or vice versa; cf. [42]). Form these matrixes, the model accuracy (i.e., the ratio between the number of features corresponding to a given SHS correctly classified and the total number of features to be associated to the above-mentioned SHS) were derived and used to evaluate the results of the classification.

Table 3. Results of the hierarchical clustering (HC) procedure.

Features used as an input of the HC algorithm	**Number of features used**	**Model accuracy (%)**
All the features in the time domain (T)	3	m.c.(*)
All the features in the frequency domain (F)	3	63%
All the features in the time-frequency domain (TF)	3	m.c
T+F	6	m.c
F+FT	6	m.c
T+FT	6	m.c
T+F+TF	9	m.c
Feature # 2	1	72%
Feature # 2, and 9	**2**	**84%**
Feature # 2, 3, and 9	3	80%
Feature # 2, 3, 5, and 9	4	78%
Feature # 2, 3, 5, 6, and 9	5	67%
Feature # 1, 2, 5, 6, 8, and 9 *Feature # 1, 2, 3, 6, 8, and 9* *Feature # 1, 2, 3, 5, 6, and 8*	6	66%
Feature # 1, 2, 4, 5, 7, and 9	6	71%
Feature # 1, 2, 3, 5, 6, 8, and 9	7	66%
(*) m.c.: misclassification		

Based on Table 3, it is possible to state the relationship between AR (through the indicators shown in Table 1) and SHS (unknown). For example, when features 2 and 9 in Table 1 (i.e., time lag and energy) were used, 84 cases out of 100 cases were correctly classified (best set of features: Δt & $Eng_{CWCs,max}$).

5. CONCLUSIONS

A non-destructive, acoustic, feature-based SHM method was presented in this paper. The validation of the proposed method was carried out through a specifically designed experimental investigation. In particular, the proposed method was applied to an asphalt concrete pavement and a change of its structural health status over time was simulated (generation and propagation of cracks): i) three lines of drilled holes were created into the pavement under test to simulate the cracks that usually are generated by vehicular traffic along the wheel paths; ii) a Light Weight Deflectometer (LWD) was used as "pilot-source" to load the pavement; iii) the acoustic responses (acoustic signals) of the pavement to the load were detected by an insulated microphone; iv) the signals were analysed through different graphical representations obtained using different mathematical tools in three domains (i.e., time, frequency, and time-frequency domains); v) different features were extracted and analysed, using a hierarchical clustering procedure and confusion matrixes, in order to understand which feature is the most meaningful in recognizing the presence and the growth over time of cracks in the monitored structure. Results show that it is possible to identify and quantify cracks into asphalt concrete road pavement using the proposed acoustic response and feature-based SHM method. Future research will focus on the improvement of the proposed method in terms of measurement system, signal analysis, in the pursuit of classifying different types of road pavements and structures based on their acoustic response.

6. REFERENCES

1. F.A. Marcianò, G. Musolino, A. Vitetta, "*Signal setting optimization on urban road transport networks: The case of emergency evacuation*", Saf. Sci., (2015) doi:10.1016/j.ssci.2014.08.005

2. F.G. Praticò, "*On the dependence of acoustic performance on pavement characteristics*", Transp. Res. Part D Transp. Environ., (2014) doi:10.1016/j.trd.2014.04.004

3. F.G. Praticò, A. Moro, R. Ammendola, "*Modeling HMA Bulk Specific Gravities: a Theoretical and Experimental Investigation*", Int. J. Pavement Res. Technol., (2) 115–122 (2009)

4. F.G. Praticò, A. Moro, R. Ammendola, "*Factors affecting variance and bias of non-nuclear density gauges for PEM and DGFC*", Balt. J. Road Bridg. Eng., (4) 99–107 (2009)

5. F.G. Praticò, A. Moro, R. Ammendola, "*Potential of fire extinguisher powder as a filler in bituminous mixes*", J. Hazard. Mater., (2010) doi:10.1016/j.jhazmat.2009.08.136

6. J. Ba, C. Su, Y. Li, S. Tu, "*Characteristics of heat flow and geothermal fields in Ruidian, Western Yunnan Province, China*", Int. J. Heat Technol., (2019) doi:10.18280/ijht.360407

7. J. Guerrero-Ibáñez, S. Zeadally, J. Contreras-Castillo, "*Sensor technologies for intelligent transportation systems*", Sensors (Switzerland), (2018) doi:10.3390/s18041212

8. S. Cafiso, C. D'Agostino, E. Delfino, A. Montella, "*From manual to automatic pavement distress detection and classification*", in 5th IEEE Int. Conf. Model. Technol. Intell. Transp. Syst. MT-ITS 2017 - Proc., (2017) doi:10.1109/MTITS.2017.8005711

9. Y. Zhang, C. Chen, Q. Wu, Q. Lu, S. Zhang, G. Zhang, Y. Yang, "*A kinect-based approach for 3D Pavement surface reconstruction and cracking recognition*", IEEE Trans. Intell. Transp. Syst., (in press) (2018)
10. K. Chen, M. Lu, X. Fan, M. Wei, J. Wu, "*Road condition monitoring using on-board three-axis accelerometer and GPS sensor*", in Proc. 2011 6th Int. ICST Conf. Commun. Netw. China, CHINACOM 2011, (2011) doi:10.1109/ChinaCom.2011.6158308
11. T. Bills, R. Bryant, A.W. Bryant, "*Towards a frugal framework for monitoring road quality*", in 2014 17th IEEE Int. Conf. Intell. Transp. Syst. ITSC 2014, (2014) doi:10.1109/ITSC.2014.6958175
12. C.W. Yi, Y.T. Chuang, C.S. Nian, "*Toward Crowdsourcing-Based Road Pavement Monitoring by Mobile Sensing Technologies*", IEEE Trans. Intell. Transp. Syst., (2015) doi:10.1109/TITS.2014.2378511
13. M.R. Carlos, M.E. Aragon, L.C. Gonzalez, H.J. Escalante, F. Martinez, "*Evaluation of Detection Approaches for Road Anomalies Based on Accelerometer Readings--Addressing Who's Who*", IEEE Trans. Intell. Transp. Syst., (2018) doi:10.1109/TITS.2017.2773084
14. C. Lenglet, J. Blanc, S. Dubroca, "*Smart road that warns its network manager when it begins cracking*", Inst. Eng. Technol. Intell. Transp. Syst., (11) 152–157 (2017) doi:10.1049/iet-its.2016.0044
15. R. Fedele, M. Merenda, F.G. Praticò, R. Carotenuto, F.G. Della Corte, "*Energy harvesting for IoT road monitoring systems*", Instrum. Mes. Metrol., (17) 605–623 (2018) doi:10.3166/I2M.17.605-623
16. W. Uddin, "*An Overview of GPR Applications for Evaluation of Pavement Thickness and Cracking*", in 15th Int. Conf. Gr. Penetrating Radar - GPR 2014, (2014)
17. M.M. Reda Taha, A. Noureldin, J.L. Lucero, T.J. Baca, "*Wavelet transform for structural health monitoring: A compendium of uses and features*", Struct. Heal. Monit., (2006) doi:10.1177/1475921706067741
18. N. Hassan, S. Mathavan, K. Kamal., "*Road crack detection using the particle filter*", in IEEE ICAC 2017, (2017)
19. M. Salman, S. Mathavan, K. Kamal, M. Rahman, "*Pavement crack detection using the Gabor filter*", in IEEE Conf. Intell. Transp. Syst. Proceedings, ITSC, (2013) doi:10.1109/ITSC.2013.6728529
20. T.A. Carr, M.D. Jenkins, M.I. Iglesias, T. Buggy, G. Morison., "*Road crack detection using a single stage detector based deep neural network*", in IEEE EESMS 2018, (2018)
21. X. Wang, Z. Hu, "*Grid-based pavement crack analysis using deep learning*", in 2017 4th Int. Conf. Transp. Inf. Safety, ICTIS 2017 - Proc., (2017) doi:10.1109/ICTIS.2017.8047878
22. P. Subirats, J. Dumoulin, V. Legeay, D. Barba, "*Automation of pavement surface crack detection using the continuous wavelet transform*", in Proc. - Int. Conf. Image Process. ICIP, (2006) doi:10.1109/ICIP.2006.313007
23. Y.O. Ouma, M. Hahn, "*Wavelet-morphology based detection of incipient linear cracks in asphalt pavements from RGB camera imagery and classification using circular Radon transform*", Adv. Eng. Informatics, (2016) doi:10.1016/j.aei.2016.06.003
24. S.W. Katicha, G. Flintsch, J. Bryce, B. Ferne, "*Wavelet denoising of TSD deflection slope measurements for improved pavement structural evaluation*", Comput. Civ. Infrastruct. Eng., (2014) doi:10.1111/mice.12052
25. J. Gajewski, T. Sadowski, "*Sensitivity analysis of crack propagation in pavement bituminous layered structures using a hybrid system integrating Artificial Neural Networks and Finite Element Method*", Comput. Mater. Sci., (2014) doi:10.1016/j.commatsci.2013.09.025

26. H. Hasni, A.H. Alavi, K. Chatti, N. Lajnef, "*A self-powered surface sensing approach for detection of bottom-up cracking in asphalt concrete pavements: Theoretical/numerical modeling*", Constr. Build. Mater., (2017) doi:10.1016/j.conbuildmat.2017.03.197
27. Y.H. Huang, "*Pavement Analysis and Design*", (2003)
28. R. Fedele, F.G. Praticò, R. Carotenuto, F.G. Della Corte, "*Damage detection into road pavements through acoustic signature analysis: First results*", in 24th Int. Congr. Sound Vib. ICSV 2017, (2017)
29. R. Fedele, F.G. Pratico, R. Carotenuto, F.G. Della Corte, "*Instrumented infrastructures for damage detection and management*", in 5th IEEE Int. Conf. Model. Technol. Intell. Transp. Syst. MT-ITS 2017 - Proc., (2017) doi:10.1109/MTITS.2017.8005729
30. ASTM E2583-07, "*Standard Test Method for Measuring Deflections with a Light Weight Deflectometer (LWD)*", ASTM International, West Conshohocken, PA, 2015, www.astm.org, (2015)
31. C.W. Schwartz, Z. Afsharikia, S. Khosravifar, "*Standardizing lightweight deflectometer modulus measurements for compaction quality assurance*", (2017). https://www.roads.maryland.gov/OPR_Research/MD-17-TPF-5-285-LWD_REPORT.pdf
32. C. Senseney, M. Mooney, "*Characterization of Two-Layer Soil System Using a Lightweight Deflectometer with Radial Sensors*", Transp. Res. Rec. J. Transp. Res. Board, (2011) doi:10.3141/2186-03
33. A.F. Elhakim, K. Elbaz, M.I. Amer, "*The use of light weight deflectometer for in situ evaluation of sand degree of compaction*", HBRC J., (2014) doi:10.1016/j.hbrcj.2013.12.003
34. F. Finn, C.L. Saraf, R. Kulkarni, K. Nair, W. Smith, A. Abdullah, "*Development of pavement structural subsystems*", (1986)
35. A.G. Bendat, J.S. Piersol, "*Random Data Analysis and Measurement Procedures*", Meas. Sci. Technol., (2000) doi:10.1088/0957-0233/11/12/702
36. E. Schubert, J. Wolfe, "*Timbral brightness and spectral centroid*", Acta Acust. United with Acust., (92) 820–825 (2006)
37. P. Kumar, E. Foufoula-Georgiou, "*Wavelet analysis for geophysical applications*", Rev. Geophys., (1997) doi:10.1029/97RG00427
38. H. Kim, H. Melhem, "*Damage detection of structures by wavelet analysis*", Eng. Struct., (2004) doi:10.1016/j.engstruct.2003.10.008
39. A. Alhasan, D.J. White, K. De Brabanterb, "*Continuous wavelet analysis of pavement profiles*", Autom. Constr., (2016) doi:10.1016/j.autcon.2015.12.013
40. M. Abdolmaleki, M. Tabaei, N. Fathianpour, B.G.H. Gorte, "*Selecting optimum base wavelet for extracting spectral alteration features associated with porphyry copper mineralization using hyperspectral images*", Int. J. Appl. Earth Obs. Geoinf., (2017) doi:10.1016/j.jag.2017.02.005
41. Mathworks, "*Hierarchical Clustering*", (2006). https://it.mathworks.com/help/stats/hierarchical-clustering.html
42. D.M. Powers, "*Evaluation: from precision, recall and F-measure to ROC, informedness, markedness and correlation*", J. Mach. Learn. Technol., (2011)